Design of a Tensegrity Servo-Actuated Structure for Civil Applications

Design of a tensegrity servo-actuated structure for civil applications

Cecilia Scoccia
Department of Industrial Engineering and Mathematical Sciences
Università Politecnica delle Marche
Ancona, 60131
Italy
Email: c.scoccia@staff.univpm.it

Giacomo Palmieri
Department of Industrial Engineering and Mathematical Sciences
Università Politecnica delle Marche
Ancona, 60131
Italy
Email: g.palmieri@staff.univpm.it

Massimo Callegari
Department of Industrial Engineering and Mathematical Sciences
Università Politecnica delle Marche
Ancona, 60131
Italy
Email: m.callegari@staff.univpm.it

Marco Rossi
Department of Industrial Engineering and Mathematical Sciences
Università Politecnica delle Marche
Ancona, 60131
Italy
Email: m.rossi@staff.univpm.it

Luca Carbonari
Department of Mechanical and Aerospace Engineering
Politecnico di Torino
Torino, 10129
Italy
Email: luca.carbonari@polito.it

Placido Munafò
Department of Construction, Civil Engineering and Architecture
Università Politecnica delle Marche
Ancona, 60131
Italy
Email: p.munafo@staff.univpm.it

Francesco Marchione
Department of Construction, Civil Engineering and Architecture
Università Politecnica delle Marche
Ancona, 60131
Italy
Email: p.munafo@staff.univpm.it, f.marchione@pm.univpm.it

Gianluca Chiappini
eCampus telematic University
Novedrate, 22060
Italy
Email: gianluca.chiappini@uniecampus.it

The use of glass elements in civil engineering is spreading in the last years beyond merely aesthetic functions for their ease of installation and production. Nonetheless, the structural performance of such materials in any condition of use is object of investigation. In this scenario, the paper analyses the performance of an innovative concept of tensegrity floor (Patent no 0001426973) characterized by a particular steel-glass adhesive junction that permits a profitable structural cooperation between such basically different materials. As known, at the base of the effectiveness of tensegrity structures lies the correct tensioning of metal strands which are devoted at keeping the rigid elements compressed. The tensioning level is then responsible of the actual deformation of the structure, which is of course of uttermost importance while speaking of civil applications. To address this issue with the adequate level of confidence required by construction practice, a mechatronic servo-system is proposed, aimed at maintaining, and modifying when needed, the stress state of the metal cables to adjust the deformation of the upper plane in response to varying loads. Three different actuation schemes, with different levels of realization complexity, are analysed and compared in simulated environment by means of a hybrid multibody-finite elements model.

Keywords: tensegrity structure, servo-actuated structure, multibody analysis, mechatronic system control

1 INTRODUCTION

Notwithstanding the low weight and versatility, the use of tensegrity structures in engineering practice has been limited till now for their peculiar complexity. Firstly, the stability conditions are extremely hard to meet. Moreover, the flexible nature often restricts their application to civil constructions. Such feature however makes them particularly feasible for mechanical and aerospace applications, where effectiveness in terms of both weight and size is required [1, 2].

Tensegrity concepts also found many applications in the field of robotics [3], where they have been mostly exploited for their large deformation characteristics [4, 5]. As obvious, the interest aroused by such application also pushed the research on the study of models for static and dynamic stability analysis, and on the actuation and control of tensegrity systems: mathematical models for the static analysis are presented in [6]; Schmalz and Agrawal [7] addressed the control and dynamic workspace determination of planar active tensegrity; Wu and Dai [8] used a screw theory approach for the rigidity and prestress stability analysis of a novel tensegrity structure (Ortho-Triplex). Machine learning, adaptive control, model based controls are just some examples of the automation practice concepts which have been applied to tensegrity robotic mechanisms [9–11]. Among others, Liu et al. proposed a novel tensegrity deployable robot for space applications based on cables and springs [12]. Shintake et al. exploited the light weight characteristics of tensegrity structures for the realization of a bio-inspired robot fish for under water applications [13]. Tensegrity mechanisms found application even in the field of robotic manipulation, for the intrinsic soft nature of the resulting structures, and the high dexterity deriving from the significant possible deformations [14]. As an example, Muralidharan and Wenger [15] studied two different types of actuated tensegrity joints for lightweight manipulators. Hong Park [16] used a tensegrity architecture for realizing an innovative large-scale additive manufacturing device. In the field of civil constructions, the research focused on control and assessment of vibrations [17, 18] and of equilibrium under varying loads [19, 20] as it is done in this manuscript for an innovative tensegrity floor.

The *Tensegrity Floor* [21, 22] object of this study (shown in Fig. 1) is a hybrid glass-metal structure characterized by a light-weight metallic sub-frame sustaining a glass floor decking. Due to its peculiar transparency, the floor particularly fits those applications where a low visual impact is preferable, as in the case of coverage of archaeological sites and the revitalizing of historical buildings. The metallic subframe is built exploiting concepts typical of tensegrity structures, historically used for their aesthetic value by architects [23, 24]. According to Renè Motro these are "*systems in a stable selfstress state, they include a discontinuous set of compressed components inside a continuum of tensioned components*" [25].

The main novelty of this tensegrity structure is the introduction of the glass plates constituting the decking as structural elements. In fact, even if the widespread glazing façades are called *structural*, the glass panels neither provide any beneficial effect to the whole building resistance, nor they are considered to contribute to the metallic underlying support structure. In the proposed solution, thanks to the designed adhesive joints, the glass is no longer in the simply-supported configuration, but it guarantees an actual contribution towards the reduction of the deformations of the whole system within the limits imposed by building codes.

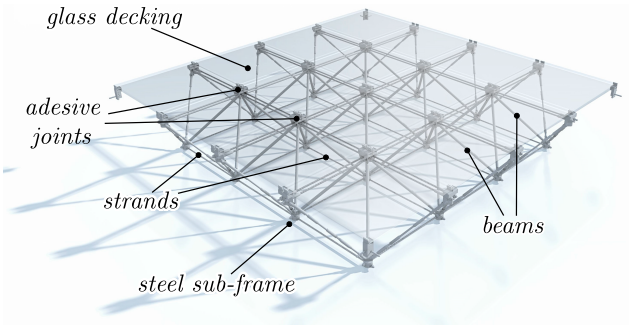

Fig. 1. THE TENSEGRITY FLOOR (PATENT N.0001426973).

Despite the beneficial effects of the innovative mounting strategy used for the slab, the resistance offered by the glass decking is not sufficient to guarantee the stability of the floor. To this purpose, the steel sub-frame must actively contribute to sustain the glass surface and to reduce the internal actions which take place in the adhesive connections. Therefore, the internal stress state of the structure shall be modified accordingly (and consequently) to the load acting on the structure.

This article presents the design of a mechatronic system conceived to realize a floor feedback control: the aim is to dynamically vary the tension of the cables by actuators in order to compensate for the measured deformation of the floor for different load conditions. First, the behavior of the floor is studied in a simulated environment by a rigid-elastic hybrid model (Section 2). The design of the mechatronic system for the actuation and control of the tensegrity structure is then presented in Section 3. In parallel with this study, the construction of a scale prototype of the tensegrity floor is under realization; Section 4 will describe the main features of the prototype and will present some preliminary results of experimental tests aimed at verifying the structural stability of the system. Finally, section 5 provides conclusions and perspectives on future work.

2 RIGID-ELASTIC HYBRID MODEL

Tensegrity structures are usually affected by large displacements depending on the internal stress of the strands. Such displacements are mainly due to the kinematics of the system rather than the deformations of the bodies themselves, with the exception of the wires of course. This simple observation is supported by the common practice, and also justified by the strain conditions of the components which usually are compressed beams and stretched cables [26, 27]. Thus, an effective modelling strategy must take into consid-

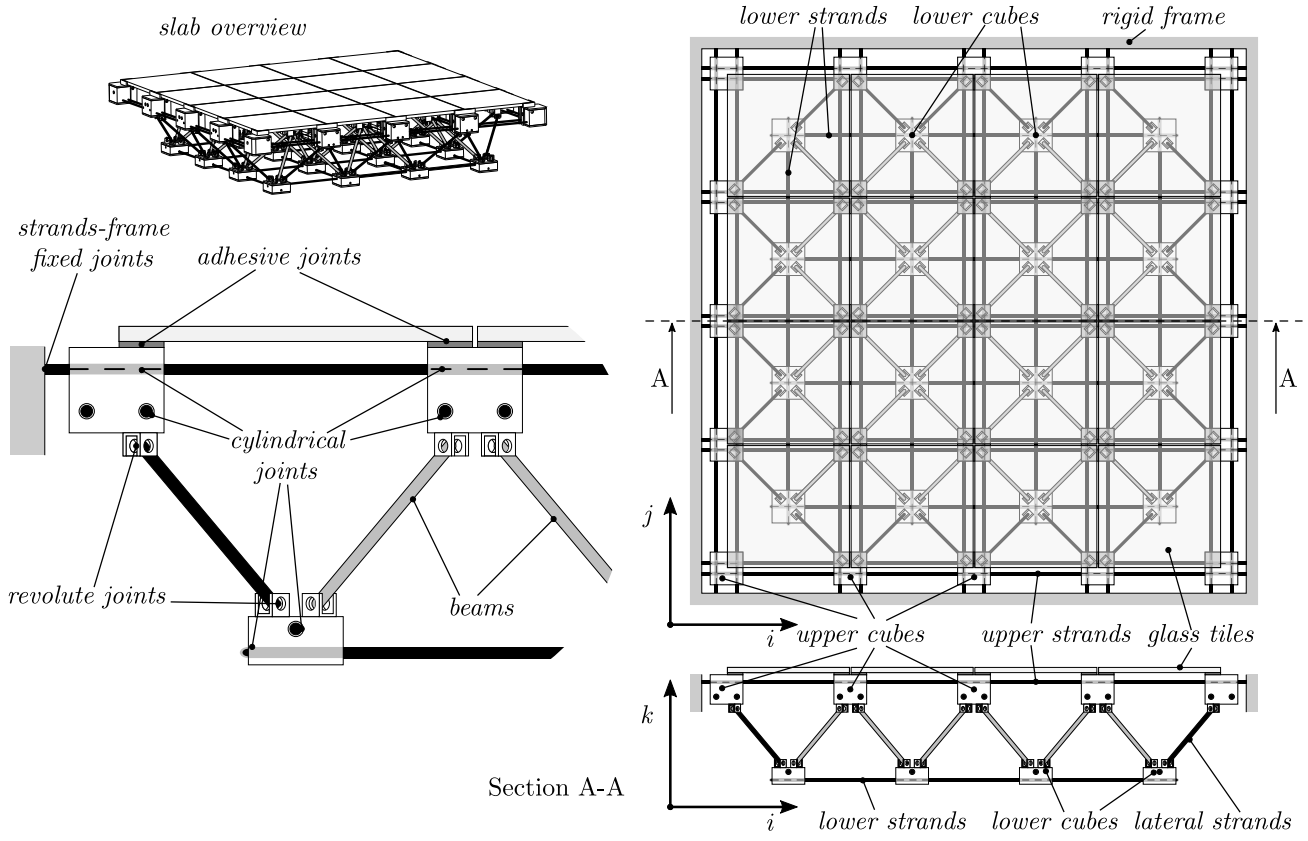

Fig. 2. BODIES AND JOINTS OF THE TENSEGRITY FLOOR.

eration such assumption by limiting the analysis of deformations to those elements which are more subject to them, and focusing on the constraint topology that makes the deflections possible. Due to these considerations a hybrid multibody-finite element approach is proposed herein for the study of the tensegrity floor. The paper describes the used modelling approach and the analyses that have been performed in an appropriate software environment.

It is worth remarking that structures for civil engineering applications are commonly strongly over-constrained, as is the proposed system. Thus, the main focus of the paper is to figure out a possible layout for controlling deformations and relieving internal stress on the most fragile elements, i.e., the glass tiles.

2.1 Rigid Bodies

The behaviour of the floor is investigated by means of a model developed in MSC.ADAMS environment according to the functional scheme shown in Fig. 2. With exception of the metal cables (indicated in figure as *upper*, *lower*, and *lateral strands*) all the bodies were built up as rigid bodies. The analyses discussed in this manuscript are aimed at the design of a small scale prototype. Therefore the dimensions and the number of elements are limited at those expected for such test rig.

To justify the choice of maintaining the mentioned bodies rigid, some results are anticipated here to provide the readers with a scale for the forces soliciting each body. The main rigid components of the tensegrity floor are:

- the *glass tiles* (sixteen in total) which represent the upper surface of the floor and are connected to the sub-frame by adhesive joints, whose model is described in the following (maximum force at each support $\sim 200\,\mathrm{N}$);
- twentyfive supporting elements of the tiles, to which they are connected, shaped as hollow steel cubes (*upper cubes* in Fig. 2, maximum force acting $\sim 400\,\mathrm{N}$);
- thirtysix rigid *beams* connected to the upper and the lower cubes by means of a spherical and a universal joint respectively (maximum axial force $\sim 400\,\mathrm{N}$);
- sixteen hollow cubes (*lower cubes*), similar to the upper ones and connected to them by the beams (maximum force $\sim 400\,\mathrm{N}$).

Mass and inertial parameters for these bodies are collected in Tab. 1. Alongside with the solid elements just introduced, a total number of forty metal cables complete the tensegrity floor by interfacing with rigid elements as described in the following.

2.2 Metal Cables

As shown in Fig. 2, the metal strands of the tensegrity floor are disposed according to a quite complex layout. In the scheme, the wires are divided into three different types, namely *lower*, *upper*, and *lateral strands*, depending on their

Table 1. PHYSICAL PROPERTIES OF RIGID BODIES.

Body	**Density**	**Mass**	**Inertia**
	kg/m^3	kg	$\times 10^{-3}\,kg\,m^2$
U.Cubes	7801	2.42	4.48, 3.84, 3.83
L.Cubes	7801	0.60	0.92, 0.53, 0.53
Beams	7801	0.12	0.20, 0.20, 0.0018
Tiles	2595	1.40	21.0, 10.5, 10.5

position within the steel sub-frame of the floor. Each type of strand plays a different role in the statics equilibrium of the structure. Qualitatively, their functions can be described as it follows:

- *upper strands*: such class of cables is devoted to keeping the upper cubes in the nodal positions of the grid they define just under the glass decking; the connection among cubes and strands is discussed later. Although the cubes are suspended on them, these cables are not sufficient to maintain a planar surface for the glass tiles without the sustain coming from the beams underneath.
- *lower strands*: the lower level of cables defines the mutual position of the lower cubes and, consequently, the actual height of the steel-subframe. In practice, the more the lower strands are strained, the closer the lower cubes are. The inclination of the beams modifies accordingly providing support to the upper cubes.
- *lateral strands*: these cables are disposed exactly as the rigid beams between the upper and the lower cubes. Their stress state affects the position of the lower cubes as done by the lower strands, but in a more complex manner. From the one hand, the higher the strain, the farer the lower cubes are pulled reducing the inclination of the beams and the resulting sustain provided to the upper cubes. From the other, the length of the lateral cables directly affects the height of the lower cubes with respect to the upper: then, the more these strands are strained, the more the lower cubes are pushed upwards providing further support to the glass decking. As shown in the next sections, this effect is the most relevant and it can be exploited to control the deformation of the whole floor.

The connections among the cubes (both upper and lower) and the strands are allowed by the holes which are drilled on the faces of the hollow blocks, through which the cables are inserted. Thanks to such connection, each cube can both rotate around and translate along the axis of the respective cable, realizing two cylindrical joints (one per each face crossed by the strand).
As aforementioned, the strands were modelled as finite element components in order to take into consideration the effect of their deformation on the mutual positions of the floor rigid elements. For their modelling, beam elements of uniform circular section were used, with a number of nodes sufficient to correctly represent the kinematics of the system. In particular, a node was placed at every cylindrical joint to transmit the constraint forces to the axes of the metal cables. The material was chosen to provide the orthotropic beams behaviour typical of metal cables. Details are provided in Tab. 2.

Table 2. MECHANICAL PROPERTIES OF THE METAL CABLES.

Parameter	**Value**	
Density	7801	kg/m^3
Young's Modulus	207	GPa
Shear Modulus	10	GPa
Poisson's Ratio	0.3	
Cable Radius	5	mm
Maximum Load	18000	N

Table 3. ELASTIC PROPERTIES USED IN THE FEM MODEL.

Material	**Young's Mod.** [GPa]	**Poisson's Ratio**
Temp. Glass	70	0.22
PVB	14.8	0.48
Steel	200	0.33
3M 7260	3	0.35

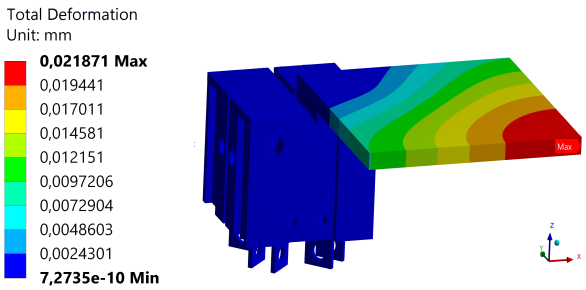

Fig. 3. FEM ANALYSIS OF JOINT DEFORMATION.

2.3 Adhesive Joints

In the design of the full scale tensegrity floor, each glass tile that composes the decking surface is connected to four cubes by means of adhesive joints, realized with structural epoxy resin. The selected material for the joints is the 3M 7260, whose mechanical properties are summarized in Tab. 4. The connection is geometrically shaped as a thin square layer ($30\,mm \times 30\,mm \times 1.1\,mm$) laying between the glass tiles and the respective lower cubes. Modeling such

Table 4. MECHANICAL PROPERTIES OF THE ADHESIVE JOINTS.

Parameter	Value	
Normal Stiffness	$3.84 \cdot 10^9$	N/m
Tangent Stiffness	$8.99 \cdot 10^8$	N/m

connections as a rigid constraint between tiles and cubes would inhibit any relative motion among the involved bodies, i.e. a fixed joint which exerts three dimensional forces and torques. The resulting constraint topology would be over-abundant and it would lock any kind of relative motion between the floor bodies. Due to that, the multibody model object of this analysis replaces the adhesive connections with an equivalent set of concentrated 6-DOF elastic elements. The values of translational and rotational stiffness (also collected in Tab. 4) were computed by means of a static analysis performed with finite elements (FE) method of the adhesive layer.

The FE model was built using the commercial code ANSYS Workbench. The model represents a single module of the floor made of a steel cube, a glass tile and the glue layer. The tile is made of a laminate glass composed by two panels of 4 mm thick tempered glass separated by a thin layer of PVB, with a thickness of 0.3 mm. The elastic properties used for the different materials are listed in Tab. 3, i.e. the Young's modulus (E), the Poisson's ratio (ν) and the density (ρ). Different loading conditions were applied in different directions to extract the equivalent normal and tangent stiffness used in the multibody simulation. A glued contact was used to join the different components of the module. An example of the used FE model is reported in Fig.3 where a vertical load was applied at the end of the tile. The final equivalent stiffnesses are listed in Tab. 4.

Notwithstanding the use of non-rigid connections, the presence of four contact points for each one of the glass tiles provides the floor prototype with an extreme stiffness which prevents any significant deformation of the structure. For this reason, for the small scale prototype (and for the respective model as well) it was chosen to use a particular assembly strategy which frees the glass tiles from the torques generated by the adhesive connections. In other words, the tiles were glued to properly realized sub-elements instead of connecting them directly to the cubes. Such support elements, then, were kept free of rotating with respect to the cubes. The resulting connections can be described as elastic spherical joints which maintain the contact among tiles and cubes without constraining the mutual rotations.

3 MECHATRONIC SYSTEM

Given the resulting behaviour depicted by the multibody model of the tensegrity floor, this section proposes a mechatronic architecture for the control of the glass decking deformation.

3.1 Effect of the Metal Cables Strain

The influence of the upper, lower, and lateral strands on the deformation is analysed in this section to design an actuation strategy able to properly modify the internal stress state of the structure with the aim of reducing the vertical displacement of the upper surface.

The representations shown in Fig. 4 collect the results obtained in terms of the tiles displacements for different internal stress conditions. Such analyses were conducted without any kind of feedback control, and without any load acting on the floor. The same initial strain was provided to each cable of the same type by imposing an identical elongation, computed as:

$$\delta l = \frac{F}{EA} l_0 \tag{1}$$

where δl is the elongation of the cable, F is the desired strain force, E is the Young's modulus of the strand, and A is its cross section area. The displacements shown in the figure are amplified to make them appreciable with respect of the floor dimension.

Different levels of the tension force F were considered for each type of cables, called hereby F_U, F_L, and F_l for upper, lower and lateral cables respectively. As it can be observed, the force F_U does not affect the deformation of the plane of the floor. In fact, the vertical displacement of the tiles is almost constant for increasing values of F_U. Moreover, without external loads, both the forces on lower and lateral strands (F_L and F_l) cause an upwards displacement of the tiles as larger as higher is the force acting on them.

3.2 Feedback Control Layout

Thanks to these considerations it is possible to draw a functional scheme of the mechatronic system for deformation control. A possible solution is providing each couple of lateral strands, i.e. the two connected to the same upper cube, with a linear actuator able to modify their internal stress. This can be done at the same time for both cables using a pulley connected to the common upper cube. A functional reference scheme is shown in Fig. 5-(a). The actuators, that must be chosen in order to ensure the correct level of thrust, must also be provided with a limit-stroke for ensuring a minimum level of loads, and avoid the loss of tension. Feasible devices are lead screw linear actuators, for different reasons. Firstly, with a proper reduction gearbox, they can provide thrusts far beyond what is needed ($\sim 2000\,\mathrm{N}$). Moreover, the use of proper trapezoidal screws provides an irreversible transmission which prevents the loss of tension while the actuator is not active (i.e., they provide a self-locked transmission which can be moved only by back-actuating the corresponding motor). The control scheme used in simulations is represented in Fig. 5-(b): the displacement information ($z_{i,j}$) coming from the proprioceptive sensors of the floor is used

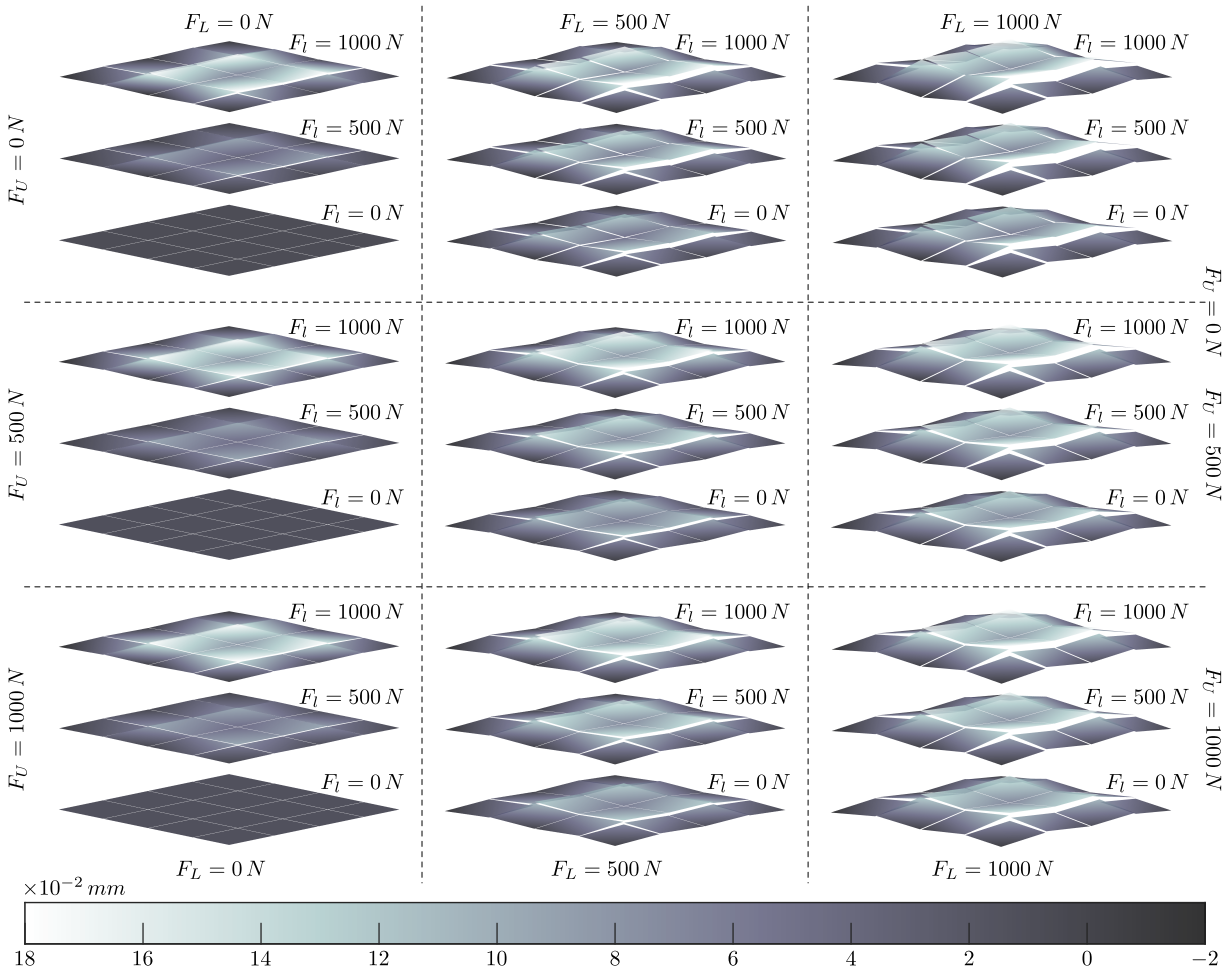

Fig. 4. BEHAVIOUR OF THE FLOOR DEFORMATION UNDER DIFFERENT COMBINATIONS OF CABLES STRAINS.

to determine a velocity set-point for the actuators (v^*). Such set-point is then followed by the actuators drivers which apply the force ($F_{i,j}$) required to restore the undeformed shape of the floor upper plane.

In this general scheme, the stroke of each actuator is controlled by means of the displacement of the cubes it directly affects with its action. Then, referring to the nomenclature introduced in Fig. 6, the forces exerted by the actuators must be defined as functions of the respective cubes vertical displacements:

$$\begin{aligned} v^*_{i,1} = v^*_{i,5} = K\sum_{j=2}^{4} z_{i,j} \;\Rightarrow\; F_{i,1} = F_{i,5} = f\left(z_{i,j}\right) \\ v^*_{1,j} = v^*_{5,j} = K\sum_{j=2}^{4} z_{i,j} \Rightarrow F_{1,j} = F_{5,j} = f\left(z_{i,j}\right) \end{aligned} \tag{2}$$

where $F_{i,j}$ is the thrust provided by the actuator connected to the lateral strand attached to the i,j lateral cube, and $z_{i,j}$ is the vertical displacement of the upper cube i,j. A visual representation of this actuation scheme, called Control Scheme 1, is given in Fig. 6(a). The proportional gain K can be calibrated accordingly to specific experimental needs. Different values have been tested in simulations; examples reported in the following of the paper are obtained setting $K = 1\,\mathrm{s}^{-1}$. The function yielding the actual force value can then be determined by means of several feedback control strategies. In the present manuscript it is chosen to use a *proportional-derivative* controller. Although the feedback architecture can be object of further detailed analysis, it is chosen here to keep it as simple as possible to leave room for observations about the mechatronic layout.

To this purpose, the next section compares the use of the control law (2) with two possibly simpler schemes which use the displacement of a single point of the floor. In fact, the main disadvantage of (2) is that of requiring the displacement measure of many control points. Even though it might look simple in a simulated environment, an actual implementation of such scheme can turn impossible in most civil applications, where the floor can be occupied by pieces of furniture, people, or any other kind of loads. Thus, it turns interesting to compare the behaviour of the control architecture when a single control point is used. To such aim, Control Scheme 2 (Fig. 6(b)) only takes into consideration the displacement of the central node:

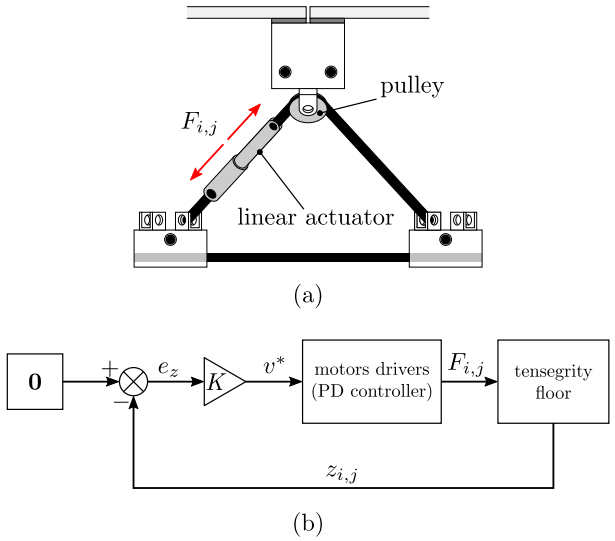

Fig. 5. (a) FUNCTIONAL SCHEME OF THE PROPOSED ACTUATION FOR THE LATERAL STRANDS; (b) PROPOSED CONTROL ARCHITECTURE.

$$\begin{aligned} v^*_{i,1} = v^*_{i,5} = Kz_{3,3} \Rightarrow F_{i,1} = F_{i,5} = f(z_{3,3}) \\ v^*_{1,j} = v^*_{5,j} = Kz_{3,3} \Rightarrow F_{1,j} = F_{5,j} = f(z_{3,3}) \end{aligned} \quad (3)$$

At last, an even simplified actuation scheme is proposed in Control Scheme 3 (Fig. 6(c)), with a reduced number of actuators. The previous schemes, in fact, made use of three actuators for every edge of the floor, for a total number of twelve actuators. The last proposed strategy uses only one actuator per edge (namely those attached to the central cubes) controlled by means of the displacements of the central node of the floor:

$$\begin{aligned} v^*_{3,1} = v^*_{3,5} = Kz_{3,3} \Rightarrow F_{3,1} = F_{3,5} = f(z_{3,3}) \\ v^*_{1,3} = v^*_{5,3} = Kz_{3,3} \Rightarrow F_{1,3} = F_{5,3} = f(z_{3,3}) \end{aligned} \quad (4)$$

It should be remarked that the system has no degrees of freedom, and all the observed measures derive from axial deformations of the strands. This fact implies a strong coupling among all the observed vertical translations, and the main aim of the following simulations is to verify whether it is possible to manage the floor deformations with a minimal set of sensors and actuators.
To test the response of the structure, a set of simulations was performed using the proposed architectures in presence and in absence of initial strains of the strands. Since the preliminary analyses showed a substantial indifference to the strain of the upper strands, only the lower cables have been analysed in this phase.

3.3 Simulations Results

The three control schemes have been tested in the simulation environment to observe their response to an external load applied to the upper surface of the glass decking. To better appreciate the dynamic behaviour, the load (red curves in plots of Fig. 7) is applied through a cubic ramp applied after equilibrium is reached. The final value of the vertical distributed load was set to $3000\,\mathrm{Nm}^{-2}$ as prescribed by the Italian building code for maximum admissible vertical loads for civil floors.
The results shown in Fig. 7 allow to draw some conclusions on the use of the different schemes. Without control of the lateral strands, the initial strain on the lower cables moves upwards the glass surface. The idea is that of exploiting this effect to reduce the burden required to the actuators to maintain the equilibrium of the floor. Actually, as witnessed by the maximum forces recorded in simulations and collected in Tab. 5, this is sharply observable only for Control Scheme 3, for which the mean thrust goes from $\sim 530\,\mathrm{N}$ to $\sim 330\,\mathrm{N}$ ($\sim 37\%$ reduction).
The better solution in terms of positioning of the upper plane is given by the Control Scheme 1 which is able to vanish the vertical displacements of all the nodes. On the contrary, both Scheme 2 and 3 present residual displacements at the end of the transient phase which cannot be corrected because of the simplified actuation laws.
The effect of the lower strain on Control Schemes 1 and 2 is negligible in terms of nodal displacements. Nonetheless, considering the forces exerted by the linear actuators (Tab. 5), a considerable beneficial influence was observed for Control Scheme 2: in that case, in fact, the mean force applied by the actuators at the end of the simulation is $\sim 279\,\mathrm{N}$ when $F_L = 0\,\mathrm{N}$, and $\sim 100N$ when $F_L = 1000N$ (reduction of $\sim 64\%$). No significant influence was observed for Scheme 1.
Although the third scheme is not able to completely assess the displacement of the floor, the performance offered when an initial strain of the lower cables is used is comparable to that of Control Scheme 2. In this case ($F_L = 1000\,\mathrm{N}$) the mean deflection of the nodes is $-4.24 \times 10^{-2}\,\mathrm{mm}$, with a peak of $-6.50 \times 10^{-2}\,\mathrm{mm}$ for the corner cubes. Control Scheme 2, in the same initial strain condition, shows a mean deflection of $-2.60 \times 10^{-1}\,\mathrm{mm}$ and a maximum of $3.24 \times 10^{-1}\,\mathrm{mm}$ again for corner cubes. In conclusion, a complete compensation of the floor surface is possible only when all the lateral strands are controlled independently (Control Scheme 1) with a significant complexity of the mechatronic system (in total 12 linear actuators) and of the measuring system (9 control nodes). Nonetheless, an acceptable result can be obtained with a much simpler approach (Control Scheme 3) which uses only 4 actuators and a single control point.

3.4 Mechatronic Layout

In order to create a control loop for the actuated tensegrity structure, a measurement system is needed to detect in real-time the deflection of the floor under varying loads.

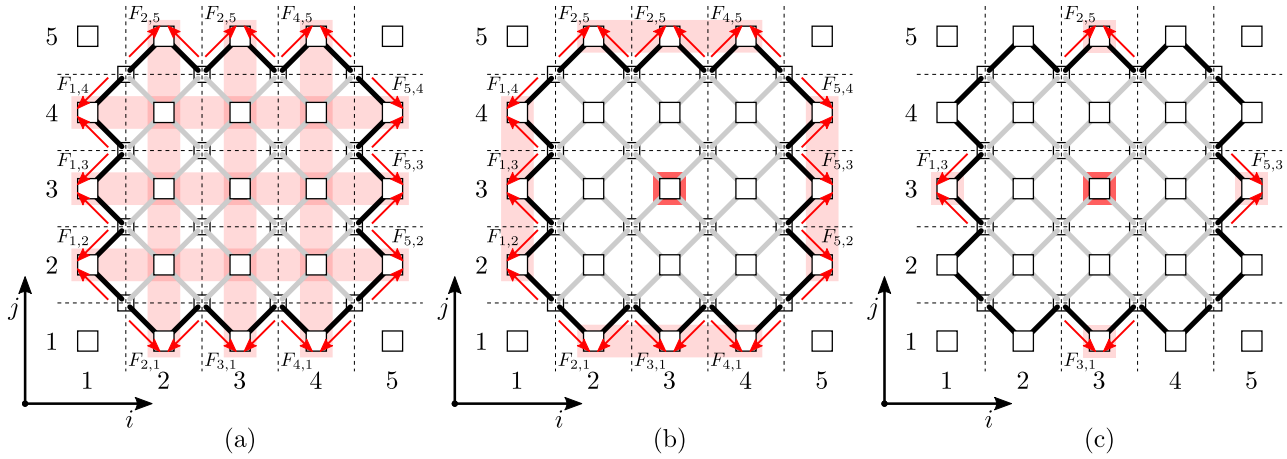

Fig. 6. TESTED FEEDBACK SCHEMES: INDEPENDENT CONTROL OF ALL LATERAL CABLES (a), CONTROL WITH REDUCED FEEDBACK DATA SET (b), AND CONTROL WITH REDUCED NUMBER OF ACTUATORS (c).

Table 5. MAXIMUM ACTUATOR FORCES FOR THE THREE CONTROL SCHEMES (C.S. IN TABLE).

Force	**C.S. 1**		**C.S. 2**		**C.S. 3**		
F_L	0	1000	0	1000	0	1000	[N]
$F_{1,2}$	153	152	252	173	–	–	[N]
$F_{1,3}$	74	75	197	105	531	327	[N]
$F_{1,4}$	228	227	414	61	–	–	[N]
$F_{5,2}$	153	152	252	173	–	–	[N]
$F_{5,3}$	74	75	197	105	531	327	[N]
$F_{5,4}$	228	227	414	61	–	–	[N]
$F_{2,1}$	90	93	201	106	–	–	[N]
$F_{3,1}$	66	67	205	99	529	339	[N]
$F_{4,1}$	222	220	408	57	–	–	[N]
$F_{2,5}$	90	93	201	106	–	–	[N]
$F_{3,5}$	66	67	205	99	529	339	[N]
$F_{4,5}$	222	220	408	57	–	–	[N]

Among contactless sensors, lasers are the best candidates to this purpose. The simplest solution is that of placing a standard laser triangulation system in an out-of-plane configuration, thus with the measuring direction orthogonal to the floor; the sensor should be placed on the ground on the bottom side of the floor, measuring the distance from a target surface fixed to the central point of the lower part of the tensegrity structure.

In case the ground on the bottom of the floor is not accessible (e.g. archaeological site or water), the out of plane configuration is not admissible, thus an alternative can be found in the scheme proposed in Fig. 8: a laser sensor in trough-beam configuration generates an analog output proportional to the amount of light measured by the receiver, thus inversely proportional to the displacement of a cursor which moves rigidly with the central point of the floor and gradually obscures the laser beam. Such kind of sensors are available up to $L = 5\,\text{m}$ maximum sensing distances, corresponding to a measurement range of $s_{max} = 16\,\text{mm}$ and a resolution of $8 \cdot 10^{-2}\,\text{mm}$ (Sensor Instruments A-LAS-24). Moreover, the bandwidth of the analog signal is 10 kHz, which makes the instrument compatible to real-time requirements of a standard control loop.

4 PRELIMINARY EXPERIMENTAL RESULTS

For the realization of the prototype, first of all the external frame was created, to which the entire structure consisting of cubes, glass plates and strands is then connected. The external support frame is made up of four IPE 120 beams welded together to form a square of size $1.20\,\text{m} \times 1.20\,\text{m}$. Holes have been drilled along the sides of the frame on which the strands are blocked. The tensegrity floor consists of two levels. The upper strands necessary to support the upper cubes are constrained to the frame at their extremities. Each cube (80 mm side) is supported by four strands. The outer cubes of the upper level are simply supported by the frame. Holes have been drilled on these cubes which are used for the passage of the strands. Cubes of the upper level are realized as shown in Fig. 9(a). The lower level is made up of cubes similar to the upper ones (with a half height), connected together by strands, and linked to the upper cubes by struts. On the lower side of the upper cubes and on the upper side of the lower cubes, perforated C-profiles have been welded to allow the connection between the two levels. The connection is made by means of struts, fixed to the C profile with appropriate bolting. For what concerns the floor, it is realized of $300\,\text{mm} \times 300\,\text{mm}$ glass tiles. The glass tiles are composed

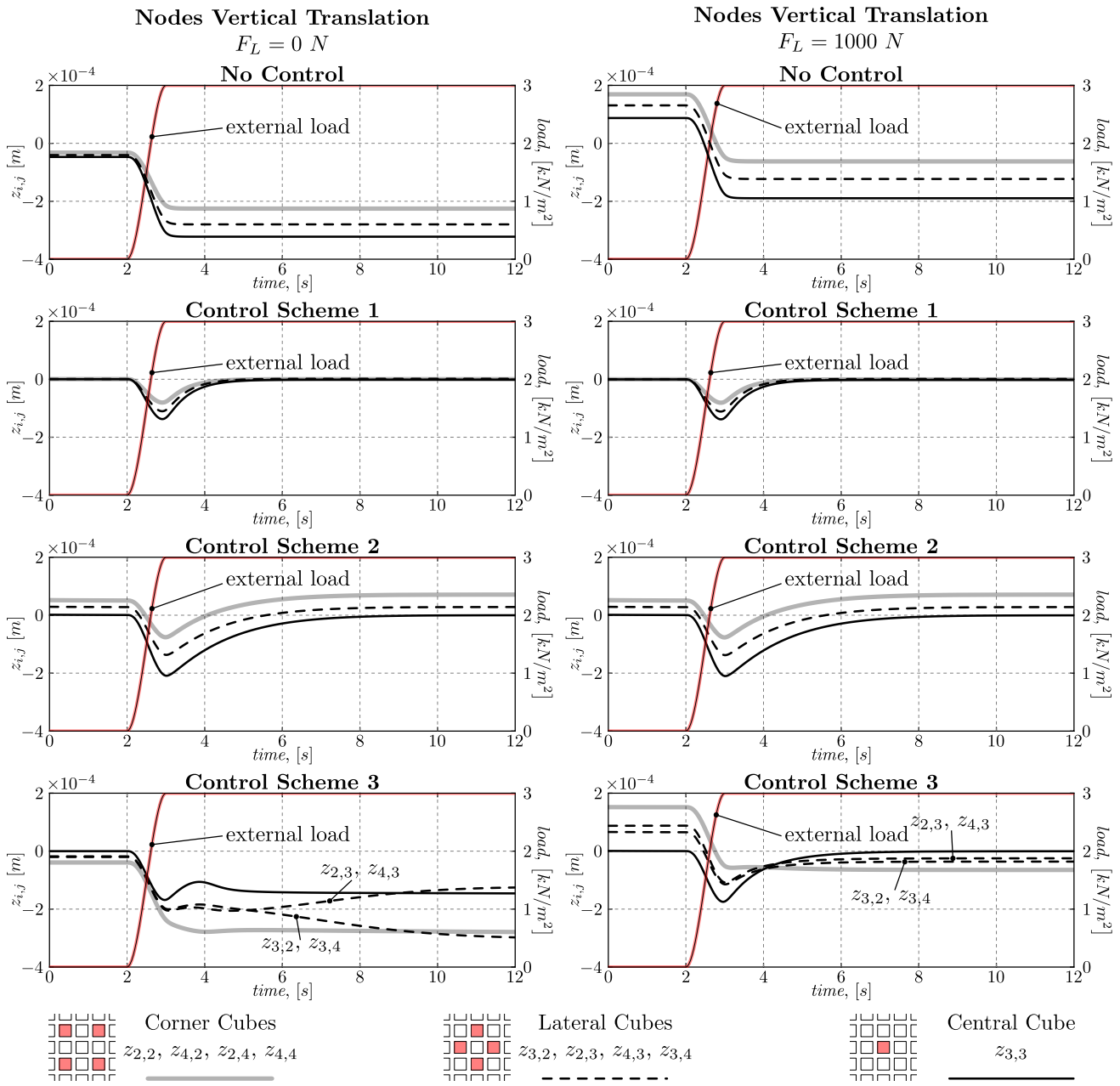

Fig. 7. TESTED FEEDBACK SCHEMES: INDEPENDENT CONTROL OF ALL LATERAL CABLES (a), CONTROL WITH REDUCED FEEDBACK DATA SET (b), AND CONTROL WITH REDUCED NUMBER OF ACTUATORS (c).

by two sheets of glass of 4 mm thickness with a 0.3 mm PVB layer interposed. Steel brackets have been glued to each corner of the glass tiles, allowing an easy connection with the supporting cubes (Fig. 9(b)). The assembled final prototype is shown in the Fig. 9(c).

4.1 Experimental test

An experimental setup to measure the displacement of the tensegrity floor under different loading conditions was developed using a photogrammetry approach. The measurement of the displacement field on the prototype is fundamental to validate the designed servo-actuated structure. In this paper, the measurement technique is described and verified under static loading conditions while the complete validation of the actuated system will be tackled in future works.

The optical grid method was used. A grid of 3×3 circular markers was glued on the upper surface of the prototype. Two digital cameras were used to capture at the same time two images of the floor at different angles. The cameras have a CMOS sensor with 1280×1024 pixel resolution (model Pixelink® B371F). The images were post-processed by image binarization and bubble analysis to get the marker centroids. Then a stereoscopic algorithm was used to derive the 3D coordinates of the markers in a global reference frame. The two cameras were suitably calibrated.

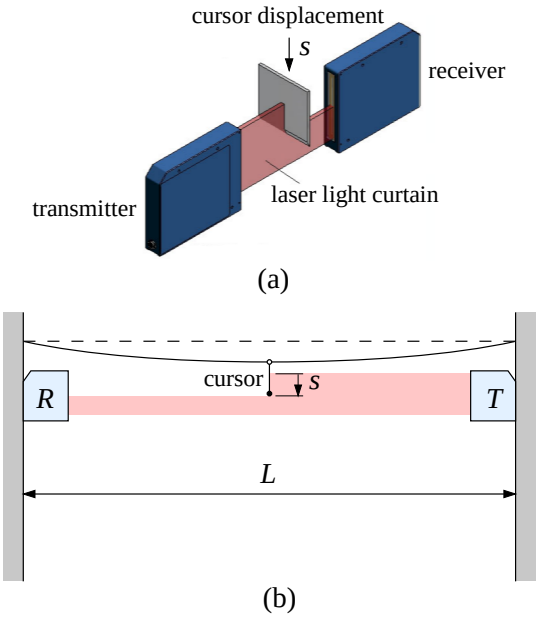

Fig. 8. FLOOR DEFLECTION MEASUREMENT SYSTEM: PRINCIPLE (a) AND FUNCTIONAL LAYOUT (b).

First, the position of the markers in the unloaded floor was obtained as reference configuration. Then the floor was loaded and the new position of the markers was derived from the stereoscopic system. Two loading conditions were taken into consideration: (i) a uniform distributed load of 400 kg, (ii) a load of 200 kg placed sideways. The tension of the cables has been set in both cases such that the floor is flat when the load is zero; then it is kept constant as the load is applied. The load was applied using a series of weights placed in the floor. When placing the weights, attention must be paid to ensure that the optical access of all markers is guaranteed.

The displacement distribution over the whole surface was eventually obtained using a bi-cubic interpolation function. The results are shown in Fig. 10, were the vertical deflection for the two loading conditions is plotted. A maximum deflection of 3.25 mm is observed at the center of the floor for the uniform load, while a maximum deflection of 2.12 mm is obtained in the sideways loading.

In order to check the accuracy of the measurement system, two displacement sensors, i.e. spring loaded linear displacement transducers (model M.A.E. PT50T), were used to measure the displacement of the loaded floor in two points distant from the circular markers. A maximum error of 4% was found in all measurement tests showing a reasonable accuracy of the interpolation function.

The adopted measurement system is rather simple and flexible, allows to obtain a reasonably accurate map of the displacement along the whole surface and can be conveniently used to validate the effect of the servo-actuated sensor. Moreover, the tests with static loads demonstrates the rigidity and the stability of the prototype.

5 CONCLUSIONS

The article studied an innovative tensegrity structure equipped by a feedback control system for compensation of deformations. The structure is modelled by a hybrid rigid-elastic model to depict the dynamic behaviour through the use of both rigid bodies and FE modelled metal cables. The influence of the initial strains of the strands is analysed and a mechatronic layout that employs linear actuators is proposed accordingly. Three different feedback control schemes of different complexity are investigated in terms of response to the application of a static load to the upper surface of the floor.

The model shows that a complete deformation assessment of the glass decking is possible only by independently actuating all the lateral strands. Nonetheless, the alternative simplified schemes offer acceptable performance both in terms of displacements of the control nodes and in terms of actuation forces.

Moreover, the feasibility of the system has been proven by the preliminary experimental tests that have been conducted on a scale prototype of the tensegrity floor. A system for the measurement of the deflection based on optical sensors is exploited to verify the response to a static vertical load. The same system will be used in future tests in order to verify the effect of a varying tension of the cables, with the aim of calibrating the control system for dynamic loads.

References

[1] Van De Wijdeven, J., and De Jager, B., 2005. "Shape change of tensegrity structures: design and control". In Proceedings of the 2005, American Control Conference, 2005., IEEE, pp. 2522–2527.

[2] Kim, T.-H., Suh, J.-E., and Han, J.-H., 2021. "Deployable truss structure with flat-form storability using scissor-like elements". *Mechanism and Machine Theory,* **159**, p. 104252.

[3] Karnan, H., Goyal, R., Majji, M., Skelton, R. E., and Singla, P., 2017. "Visual feedback control of tensegrity robotic systems". In 2017 IEEE/RSJ International Conference on Intelligent Robots and Systems (IROS), IEEE, pp. 2048–2053.

[4] Vespignani, M., Friesen, J. M., SunSpiral, V., and Bruce, J., 2018. "Design of superball v2, a compliant tensegrity robot for absorbing large impacts". In 2018 IEEE/RSJ International Conference on Intelligent Robots and Systems (IROS), IEEE, pp. 2865–2871.

[5] Vespignani, M., Ercolani, C., Friesen, J. M., and Bruce, J., 2018. "Steerable locomotion controller for six-strut icosahedral tensegrity robots". In 2018 IEEE/RSJ International Conference on Intelligent Robots and Systems (IROS), IEEE, pp. 2886–2892.

[6] Crane III, C. D., Duffy, J., and Correa, J. C., 2005. "Static Analysis of Tensegrity Structures ". *Journal of Mechanical Design,* **127**(2), pp. 257–268.

[7] Schmalz, A. P., and Agrawal, S. K., 2008. "Dynamic Workspace and Control of Planar Active Tensegritylike Structures". *Journal of Mechanical Design,* **130**(12).

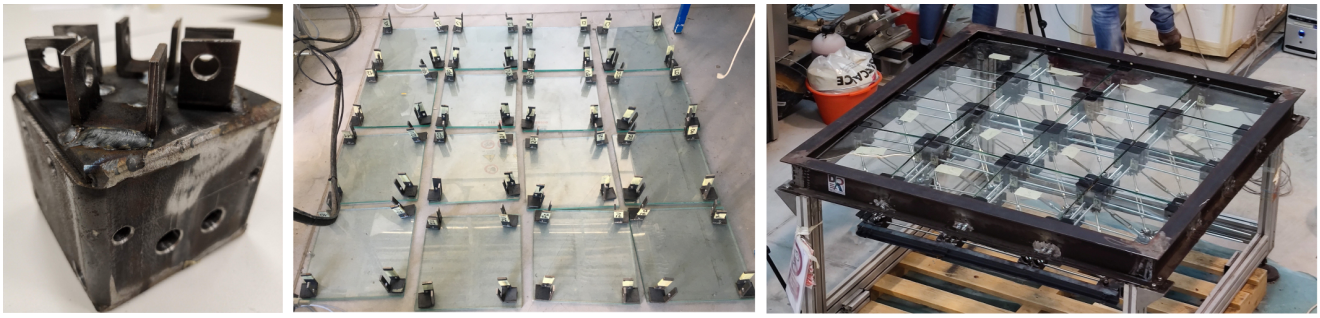

(a) (b) (c)

Fig. 9. (a) UPPER CUBE; (b) GLASS TILES WITH GLUED BRACKET; (c) ASSEMBLED PROTOTYPE.

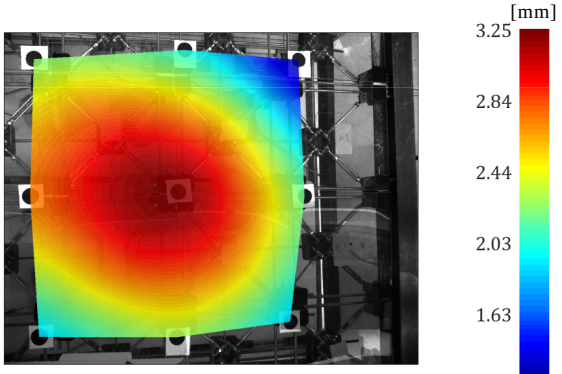

(a)

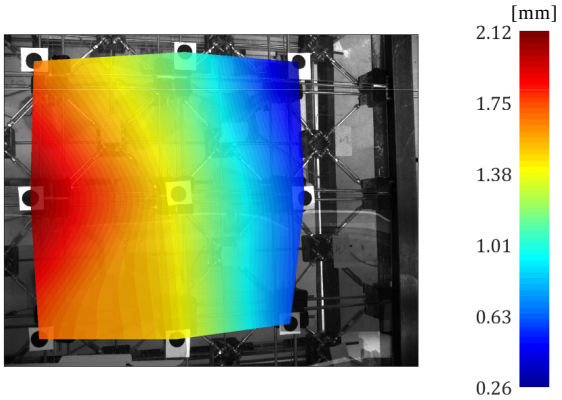

(b)

Fig. 10. VERTICAL DISPLACEMENT MAPS: (a) UNIFORM LOAD OF 400 kg ; (b) LATERAL LOAD OF 200 kg.

[8] Wu, L., and Dai, J. S., 2020. "A Novel Ortho-Triplex Tensegrity Derived by the Linkage-Truss Transformation With Prestress-Stability Analysis Using Screw Theory". *Journal of Mechanical Design,* **143**(1).

[9] Veuve, N., Sychterz, A. C., and Smith, I. F., 2017. "Adaptive control of a deployable tensegrity structure". *Engineering Structures,* **152**, pp. 14–23.

[10] Zhang, M., Geng, X., Bruce, J., Caluwaerts, K., Vespignani, M., SunSpiral, V., Abbeel, P., and Levine, S., 2017. "Deep reinforcement learning for tensegrity robot locomotion". In 2017 IEEE International Conference on Robotics and Automation (ICRA), IEEE, pp. 634–641.

[11] Wang, R., Goyal, R., Chakravorty, S., and Skelton, R. E., 2020. "Model and data based approaches to the control of tensegrity robots". *IEEE Robotics and Automation Letters,* **5**(3), pp. 3846–3853.

[12] Liu, S., Li, Q., Wang, P., and Guo, F., 2020. "Kinematic and static analysis of a novel tensegrity robot". *Mechanism and Machine Theory,* **149**, p. 103788.

[13] Shintake, J., Zappetti, D., Peter, T., Ikemoto, Y., and Floreano, D., 2020. "Bio-inspired tensegrity fish robot". In 2020 IEEE International Conference on Robotics and Automation (ICRA), IEEE, pp. 2887–2892.

[14] Ramadoss, V., Sagar, K., Ikbal, M. S., Calles, J. H. L., and Zoppi, M., 2020. "Hedra: A bio-inspired modular tensegrity soft robot with polyhedral parallel modules". *arXiv preprint arXiv:2011.14240*.

[15] Muralidharan, V., and Wenger, P., 2021. "Optimal design and comparative study of two antagonistically actuated tensegrity joints". *Mechanism and Machine Theory,* **159**, p. 104249.

[16] Hong Park, J. "Design and simulation of a large-scale 3d printing system using truncated tetrahedral tensegrity robot". In *Earth and Space 2021*. pp. 970–977.

[17] Chan, W. L., Arbelaez, D., Bossens, F., and Skelton, R. E., 2004. "Active vibration control of a three-stage tensegrity structure". In Smart Structures and Materials 2004: Damping and Isolation, Vol. 5386, International Society for Optics and Photonics, pp. 340–346.

[18] Ali, N. B. H., and Smith, I., 2010. "Dynamic behavior and vibration control of a tensegrity structure". *International Journal of Solids and Structures,* **47**(9), pp. 1285–1296.

[19] Adam, B., and Smith, I. F., 2008. "Active tensegrity: A control framework for an adaptive civil-engineering structure". *Computers & Structures,* **86**(23-24), pp. 2215–2223.

[20] Korkmaz, S., 2011. "A review of active structural control: challenges for engineering informatics". *Computers & Structures,* **89**(23-24), pp. 2113–2132.

[21] Munafò, P., 2017. Tensegrity floor, May 3. Patent

N.0001426973.

[22] Alderucci, T., Terlizzi, V., Urso, S., Borsellino, C., and Munafò, P., 2018. "Experimental study of the adhesive glass-steel joint behavior in a tensegrity floor". *International Journal of Adhesion and Adhesives,* **85**, pp. 293–302.

[23] Quirant, J., Kazi-Aoual, M., and Motro, R., 2003. "Designing tensegrity systems: the case of a double layer grid". *Engineering structures,* **25**(9), pp. 1121–1130.

[24] Cimmino, M., Miranda, R., Sicignano, E., Ferreira, A., Skelton, R., and Fraternali, F., 2017. "Composite solar façades and wind generators with tensegrity architecture". *Composites Part B: Engineering,* **115**, pp. 275–281.

[25] Motro, R., 2003. *Tensegrity: structural systems for the future*. Elsevier.

[26] Fest, E., Shea, K., and Smith, I. F., 2004. "Active tensegrity structure". *Journal of Structural Engineering,* **130**(10), pp. 1454–1465.

[27] Shibata, M., Saijyo, F., and Hirai, S., 2009. "Crawling by body deformation of tensegrity structure robots". In 2009 IEEE international conference on robotics and automation, IEEE, pp. 4375–4380.